Considerations on ejection velocity estimations from infrared radiometer data: A case study at Stromboli volcano

Laure Chevalier, Franck Donnadieu

Citation : Chevalier L., Donnadieu F., 2015. Considerations on ejection velocity estimations frominfrared radiometer data: A case study at Stromboli volcano. Journal of Volcanology and Geothermal Research 302 (2015) 130–140. http://dx.doi.org/10.1016/j.jvolgeores.2015.06.022

Considerations on ejection velocity estimations frominfrared radiometer data: A case study at Stromboli volcano

Laure Chevalier [a], Franck Donnadieu [b,*]

[a] École Normale Supérieure de Lyon, 46 allée d'Italie, 69007 Lyon, France ; laure.chevalier@univ-savoie.fr
[b] Laboratoire Magmas et Volcans, Université Blaise Pascal–CNRS–IRD, OPGC, 5 rue Kessler, 63038 Clermont-Ferrand, France
[*]Corresponding author. F.Donnadieu@opgc.fr

Received 20 January 2015 ; Accepted 17 June 2015 ; Available online 4 July 2015

Abstract

Synchronous recordings of normal Strombolian explosions with a thermal camera and infrared radiometers provide a unique opportunity to understand signals from less expensive radiometers. Using records from Stromboli volcano, we analyze in particular the limitations of using signals from infrared radiometers alone to quantify the plume ascent kinetics. We conclude that infrared radiometers pointing close to the vent, either single or coupled, are often insufficient for velocity retrieval due to the complex structure and dynamics of the plumes and their evolution with time. In addition to practical implementation difficulties in the field, this is mainly due to the rapid succession and overlapping of thermal components in the radiometer's field of view. Optimized geometries of radiometer fields of view and new retrieval methodologies are proposed to improve velocity estimates from one or coupled radiometers.

Keywords: Infrared radiometer, Thermal camera, Ejection velocity, Strombolian explosions, Plume dynamics.

1. Introduction

Geophysical monitoring of volcanic eruptions has offered great opportunities to identify and quantify controlling parameters for eruption dynamics (e.g., Kaminski and Jaupart, 2001; Carazzo et al., 2008; Mastin et al., 2009). Ejection velocity is a crucial source parameter to measure as it is directly related to the driving gas overpressure and decompression rate and controls the mode and range of pyroclast dispersal (e.g., Woods, 1995). It is thus essential for the assessment of eruption intensity and hazards.

Ejection velocity for explosive eruptions was first estimated from photoballistic techniques, that gave access to ballistic velocities and ash plume ascent velocities, and allowed plume front tracking (Chouet et al., 1974; Wilson and Self, 1980; Ripepe et al., 1993). Acoustic Doppler sounder, Doppler radar and Forward Looking Infra-red Radiometer (FLIR) camera were also used to obtain particle ejection velocities during Strombolian activity (Weill et al., 1992; Hort et al., 2003; Donnadieu et al., 2005). Velocity retrieval with FLIR camera was also used to describe more precisely eruption dynamics at Stromboli volcano (Patrick et al., 2007; Harris et al., 2012).

More recently, radiometers have been widely used for ejection velocity and plume front velocity measurements. Their low cost (one hundred to a few thousand dollars) compared with that of high-resolution high-speed thermal cameras (several tens of thousand dollars), their quick and easy implementation and data treatment, their low storage memory cost, their low energy consumption in the field and robustness make them useful tools for monitoring and for simultaneous collection of seismic and infrasonic data. They are also potentially useful for ejection velocity retrieval. Currently used radiometers have Field Of View (FOV) ranging from 0.25° to 60° aperture angle (for a review of thermal sensors, cf. Harris, 2013). This range of apertures makes it possible to use radiometers for simple plume detection (Ripepe et al., 2002; Harris and Ripepe, 2007a) and general information on the eruption dynamics, or precise temperature recording of the plume (e.g., Harris and Ripepe, 2007b; Sahetapy-Engel et al., 2008).

However, whereas velocities are relatively straightforward to obtain from thermal camera images using the pixel resolution (e.g., from particle tracking, thermal profile evolution along a line, etc.), eruption velocity estimates from infra-red (IR) radiometer data alone are more difficult to infer. Indeed, velocity estimates are based on interpretations of the radiometric signal waveform (Johnson et al., 2004; Sahetapy-Engel et al., 2008; Harris et al., 2012) which are not well defined or verified.

In this paper, we compare thermal records from radiometers and a FLIR camera, collected simultaneously at the SW and NE craters of Stromboli volcano (Fig. 1) in September–October 2012 during normal Strombolian activity. We were able to correlate the radiometric signal waveforms with eruption dynamics, and test the hypotheses used for waveform interpretation. By comparing thermal data from radiometers and thermal video cameras, we first estimate ejection velocity using current methods based on radiometric signal interpretation and show that they are not reliable in most conditions. We then discuss the meaning of ejection velocity measured with thermal sensors and we examine the sources of error in velocity retrievals using radiometers. Finally, we propose some hardware and methodological developments to improve radiometric data quality and interpretation.

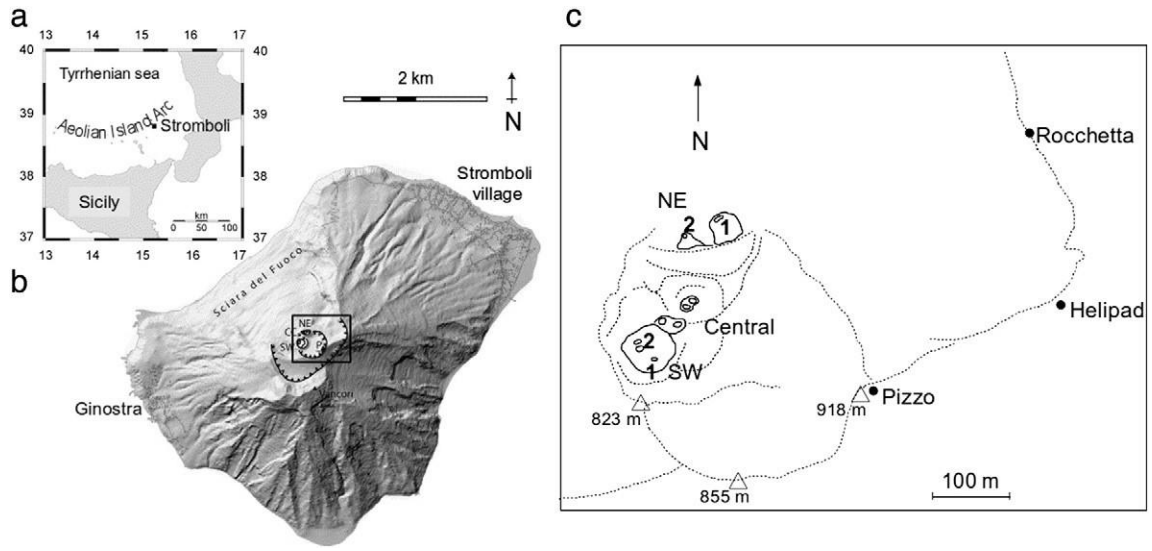

Fig. 1. Observation context. a) Location of Stromboli in Aeolian Islands and b) DEM map of Stromboli (from Harris and Ripepe, 2007a,2007b, courtesy of Anthony Finizola) and c) drawing of summit craters' actual configuration, and observation site emplacements.

2. Theory

2.1. Radiometry

Any body at a temperature above 0 K tends to cool down by emitting electromagnetic radiation. The intensity and wavelength of this radiation depend on the body's temperature T and emissivity ε (ε = 1 for black body; dimensionless). The total intensity of emitted radiation j, called radiant exitance (radiant flux emitted by a surface by unit area, W m^{-2}) of the body, is defined by the Stefan–Boltzmann law:

$$j = \sigma \varepsilon T^4 \quad (1)$$

where σ is Stefan–Boltzmann's constant (5.68 × 10^{-8} W m^{-2} K^{-4}). Radiometric thermal sensors, such as radiometers and IR cameras, detect a specific infrared range of radiation in the electromagnetic spectrum. They are able to determine a mean temperature for the emitting bodies present in their FOV, such as gas and particles from an eruptive plume. The measured temperature T_{rad} corresponds to:

$$\sigma \varepsilon T_{rad}^4 = \int_{FOV} \sigma \varepsilon T^4(x,y)\,dx\,dy \quad (2)$$

Radiometric thermal sensors usually used in volcanology are sensitive to radiation of 8–13 μm. Although the peak in spectral radiant exitance for lava at 1000 °C is at 2.2 μm, emission at magmatic temperature remains 30 to 150 times superior to that at 20 °C in the 8–13 μm domain (Wein's law), considering ε = 1 (Harris, 2013). As ash and scoria are not transparent to infrared radiation, the signal recorded by thermal sensors mainly concerns the superficial, nearby part of the plume when optical thickness is high (e.g., Wen and Rose, 1994; Gouhier et al., 2012). Besides, signal amplitude is dominated by radiation emitted by hot, dense particles that may hide weaker contribution of smaller, colder objects. This might limit precision and representativeness of signal variations.

2.2. Two-component model

Whereas particles and plume front velocities are straightforward to retrieve from FLIR camera video, by following the evolution of these components on consecutive images, radiometers only give access to a mean temperature value for the whole FOV.

To simplify radiometric signal interpretation, most studies consider a two-thermal component description of the eruption, involving a cold background and a hot plume (Johnson et al., 2004; Sahetapy-Engel et al., 2008; Harris et al., 2012). Using this approximation, Eq. (2) reduces to:

$$\sigma T_{rad}^4 = f\sigma T_h^4 + (1-f)\sigma T_c^4 \quad (3)$$

where f is the fraction of the FOV occupied by the plume, T_h is the apparent temperature of the plume, and T_c is the temperature of the background, considering that both the plume and the background are homogeneous and of constant temperature. The temperature measured by the radiometer thus depends on f, T_c and T_h. Variations of T_{rad} only depend on the way f varies:

$$\frac{df}{dt} = \frac{4T_{rad}^3}{\left(T_h^4 - T_c^4\right)} \frac{dT_{rad}}{dt}. \quad (4)$$

Assuming a two-thermal-component description of the plume, we then expect radiometric signal variations to be interpretable as plume movements in the FOV.

The radiometric signal waveform has been sequenced into several well defined and recognizable stages (Fig. 2): (i) The signal onset corresponds to the first hot particles of the plume entering the FOV. (ii) A fast increase follows the signal onset, up to a temperature maximum. This phase corresponds to the filling of the radiometer's FOV by hot material from the plume (Sahetapy-Engel et al., 2008; Harris et al., 2012). (iii) The temperature maximum associated with punctual emission is a sharp peak. The FOV is then completely filled with hot material. When the emission is sustained, the peak temperature values remain high for several seconds. Further peaks are usual in the case of additional explosive pulses. (iv) The radiometric signal then decreases as plume material cools down, scatters, and progressively exits the FOV, while the flux of material entering the FOV wanes. (v) After the decay phase, a weak increase sometimes occurs, due to fallout of hot particles onto the crater wall portion visible in the FOV, and gas and ash dissipation.

This reasonably intuitive interpretation provides access to simple methods of velocity estimation.

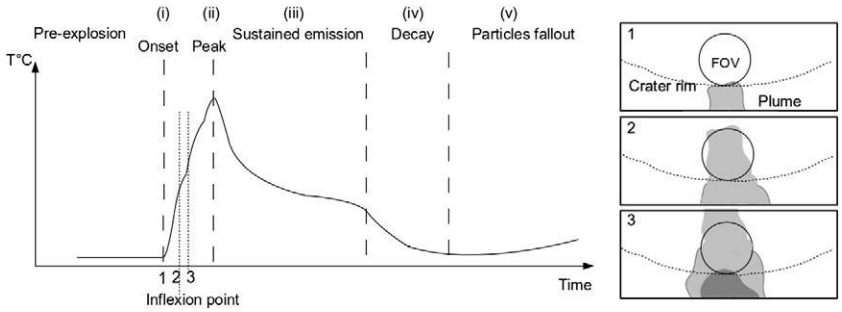

Fig. 2. Typical radiometric signal observed during Strombolian eruptions. 1) The signal onset corresponds to the first particles entering the FOV. 2) The first particles leaving the FOV generate an inflexion point. 3) The arrival of a hotter component in the FOV generates a new temperature increase.

2.3. Velocity estimation from signal waveform interpretation — current methods

Three methods based on a two-thermal-component description of the eruption have been used in past studies to retrieve velocity estimates from radiometric measurements. They assume a single, homogeneous plume, broader than the FOV's diameter, with a sharp front, and that the plume front movement is purely vertical.

The first method uses the delay time between the onset point and the peak, assuming they correspond respectively to the first arrival at the bottom of — and the exit through the top of — the FOV, of the same thermal perturbation (plume front). Knowing the FOV diameter D, the plume front velocity v_{front} (e.g., Sahetapy-Engel et al., 2008) is obtained:

$$v_{front} = \frac{D}{(t_i - t_0)} \quad (5)$$

where t_i and t_0 are the times of inflexion and onset points, respectively.

The second method uses the time delay between the signal inflexion points of two superposed radiometers (e.g., Johnson et al., 2004). In this case we consider that the onset points of both signals are due to the plume front. The velocity is then:

$$v_{front} = \frac{D'}{(t_2 - t_1)} \quad (6)$$

where D′ is the distance between the two FOVs' bottoms, t_2 is the onset time for the highest radiometer's signal, and t_1 is the onset time for the lowest one.

A third way was proposed by Johnson et al. (2004), using the derivative of the temperature increase between the onset and first inflexion points. Indeed, temperature variations are linked to variations of the FOV fraction f occupied by the plume. When it crosses the FOV:

$$\frac{df}{dt} = \frac{8 d v_{front}}{\pi (D)^2} \quad (7)$$

where d is half the width of the FOV at the plume front height. When the plume front reaches the middle of the FOV (d = D/2), df/dt is maximal and corresponds to:

$$\frac{df}{dt} = v_{front} S \quad (8)$$

where S = 4/(πD) is the ratio between the width of the apparent front plume in the FOV and the total FOV area. Then from Eq. (4) we obtain:

$$v_{front} = \frac{4 T_{rad}^3}{S\left(T_h^4 - T_c^4\right)} \frac{dT_{rad}}{dt}. \quad (9)$$

In the following, we compare the ejection velocity estimated with these three methods from radiometric signals recorded during normal Strombolian activity at Stromboli with thermal camera derived velocity.

3. Data acquisition at Stromboli

3.1. Background: Strombolian activity

Explosive magmatic degassing at Stromboli volcano is thought to be associated with the formation of pressurized gas pockets, called slugs, ascending through the magma in the conduits (Wilson, 1980; Jaupart and Vergniolle, 1989; Parfitt and Wilson, 1995; Ripepe and Gordeev, 1999; Rust and Cashman, 2004; James et al., 2006; Taddeucci et al., 2013). They burst at the free surface of the magma, releasing gas plumes from the vent with various proportions of ash and bombs, causing mild, frequent, short-lived explosive eruptions (during normal activity). Eruptive plume style varies from a high-velocity jet of gas-thrust particles to buoyantly rising ash-dominated thermals (e.g., Ripepe et al., 1993; Patrick et al., 2007).

At Stromboli, maximum pyroclast ejection velocities in the range of 20–100 m s^{-1} were first measured by means of photoballistic techniques (Chouet et al., 1974; Blackburn et al., 1976; Ripepe et al., 1993), acoustic Doppler sounder (Weill et al., 1992), Doppler radar (Hort et al., 2003; Gerst et al., 2008; Scharff et al., 2008; Harris et al., 2013), and Forward Looking Infra-red Radiometer (FLIR) camera (Patrick et al., 2007). Using FLIR images of normal Strombolian activity for 34 events at the NE crater in 2004, Harris et al. (2012) then measured near-vent velocities of up to 213 m s^{-1} (mean: 66–82 m s^{-1}) for lapillisized pyroclasts in the initial diffuse spray of particles. The spray was followed within about 0.1 s by a burst comprising a mixture of ash and lapilli but dominated by bomb-sized particles, moving at 46 m s^{-1} on average (up to 129 m s^{-1}). More recently, Taddeucci et al. (2012) captured centimeter-sized particles moving at the vent exit at maximum velocities of 172 to 405 m s^{-1} using a high-speed camera (visible) for 6 ash-free explosions at the SW crater in 2009. Also at Stromboli, Bombrun et al. (2014) measured at-vent maximum velocities of 158 to 240 m s^{-1} during normal Strombolian activity, using 200 Hz FLIR thermal videos with pixel size of 5.3 cm.

3.2. Instrumental setup

Thermal data were collected simultaneously at the SW and NE craters of Stromboli volcano (Fig. 1) between 27 September and 5 October 2012 during normal Strombolian activity (Harris et al., 2013). We used two Land/Minolta Cyclops 300 AF thermopile radiometers (−50 to 1000 °C; ±1 °C) operating in the 8–13 μm range, having a response time of 0.5 s (90%). The signal was sampled at 50 Hz by a Campbell CR1000 data logger. We also used a FLIR SC660 thermal video camera (30 Hz, 640 480 pixels) operating between 7.5 and 13.5 μm (−40 °C to 1500 °C; ±2 °C), having a detector time constant of 6 ms, i.e., the time span required for the output signal to vary from its initial value by 63% of its final change. The instruments were deployed on three observation sites (Pizzo, Helipad, Rochetta shelters), at 300 to 430 m from the

active vent, looking either into the SW crater (vent 1 mainly) or the NE crater (vent 1, Fig. 1) (see supplementary material 1 for more details). The two radiometers had a 1° FOV and the camera had an 18° by 24° FOV (IFOV: 0.65 mrad). These respectively correspond to 26– 46 m^2 and 15,000–25,700 m^2 areas for the given vent distance (Table 1). The pixel size at the vent distance ranges from 23 to 26 cm, depending on the crater targeted. The first radiometer's FOV was aimed toward the base of the plume emission so that its bottom was slightly above the crater rim. When the second radiometer was used, its FOV bottom was positioned just above the FOV of the first radiometer. The FLIR video camera's FOV was always centered on the vent, and comprised a portion of the crater flank. During data acquisition, all instruments were synchronized using GPS.

All velocities were corrected for the measurement tilt angle, as the observation sites were not at the same elevation as the vents, making vertical movements within the instrument's FOV look smaller than they actually were. Considering that observed plume movements are mostly vertical, the error was corrected by dividing velocity estimates by the cosine of the tilt angle of the instrument's line of sight (Taddeucci et al., 2012).

4. Results

4.1. Radiometric signal waveform

The radiometric signal recorded during the observed eruptions pretty looks like the theoretical 2 component associated signal. Measured temperatures were ranging from 10 °C, when the FOV was filled with cold background, up to 650 °C, during the most intense eruptions. For most of the eruptions, however, the recorded temperature did not exceed 350 °C. The points of interest for measuring plume front velocity are well defined for most of eruptions. During the ascent phase, we often observe a step-like temperature increase (Fig. 3). Looking at IR videos for the corresponding eruptions, we conclude that this is caused by the arrival of major hotter thermal components of the plume which successively fill the FOV. To apply the first method described earlier, we then used the first inflexion point (i.e., the first time the temperature increase slows down in a step-like variation) instead of the theoretical peak point, in the same way as Sahetapy-Engel et al. (2008).

4.2. Velocity estimation

We applied the three methods for velocity retrieval to all the eruptions observed with radiometers. Mean values were 6.75 m s^{-1}, 15.24 m s^{-1}, 19.38 m s^{-1} respectively with the methods using the onset-peak delay, the onset delay between two radiometers, the radiometric signal derivative (supplementary material 2).

Using the FLIR software ResearchIR, we were able to determine the FOV locations of both radiometers in the camera's FOV by calculating synthetic radiometric signal from specific FOV shapes (see Section 5.3) and comparing it with our radiometric data. We checked which thermal component caused the radiometric signal variations used for our velocity estimations. In most cases, plume fronts associated with signal onset and first inflexion point correspond to the first sub-pixel sized hot

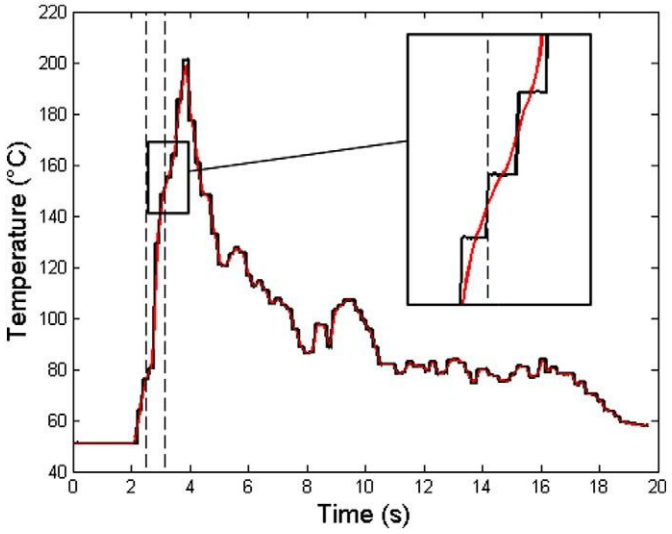

Fig. 3. Example of real radiometric signal (black curve) recorded during an eruption (30/09/12, 10:24 GMT, SW crater), with inflexion points (zoom). Thetemperature increase at the beginning of the eruption sometimes slows down, resulting in a step-like variation. These inflexion points might be caused by consecutive thermal components crossing the FOV. On the graph, inflexion points are signaled with dashed lines. They were determined from smoothed signal (red curve).

particles. From FLIR video data, the velocity of these particles was calculated and compared with velocity estimations from radiometric methods (Fig. 4).

Results from radiometric methods look very poorly correlated with IR video observations for the three methods. The slope of the best linear fit is far from 1 (no more than 0.1) and the intercept is close to the mean velocity value, for each method. Besides, all the methods give quite low velocity values for the onset phase of Strombolian eruptions compared to velocities measured by other methods (Harris et al., 2012; Patrick et al., 2007; Taddeucci et al., 2012; Bombrun et al., 2014). Looking at the normalized difference between estimation from radiometer and measurements from IR video, defined as the ratio between the velocity difference and the radiometric velocity, we find that radiometric mean error is about 390%, 209% and 143% respectively for the three methods.

Current methods to retrieve ejection velocity from radiometric signal do not give reliable results. However, we here assumed a thermally homogeneous plume with a sharp front, and a mean plume temperature significantly different from the background temperature. This may be way too simplistic with regard to reality, and lead to imprecision in the estimations. Besides, the recorded radiometric signal only concerns a small area of the plume, which may not be representative for the whole plume.

5. Discussion

5.1. Signal source — ejection velocity definition

Using ResearchIR software to compare radiometric data with IR video, we were able to analyze the eruption dynamics. The hot particles

Table 1
Acquisition parameters of radiometers and thermal cameras for each measurement configuration.

Crater	Observation site	Downward inclination (°)	Distance to vent (m)	1° radiometer FOV size (m^2)	FLIR camera FOV size (m^2)	Pixel (m^2)	Pixel length (m)
SW	Pizzo	27	315	26.6	1.50E+04	4.85E−02	2.33E−01
NE	Pizzo	29	320	28.0	1.58E+04	5.10E−02	2.41E−01
NE	Helipad	14	430	45.6	2.57E+04	8.30E−02	2.92E−01
NE	Rochetta	3	400	38.3	2.16E+04	6.98E−02	2.64E−01

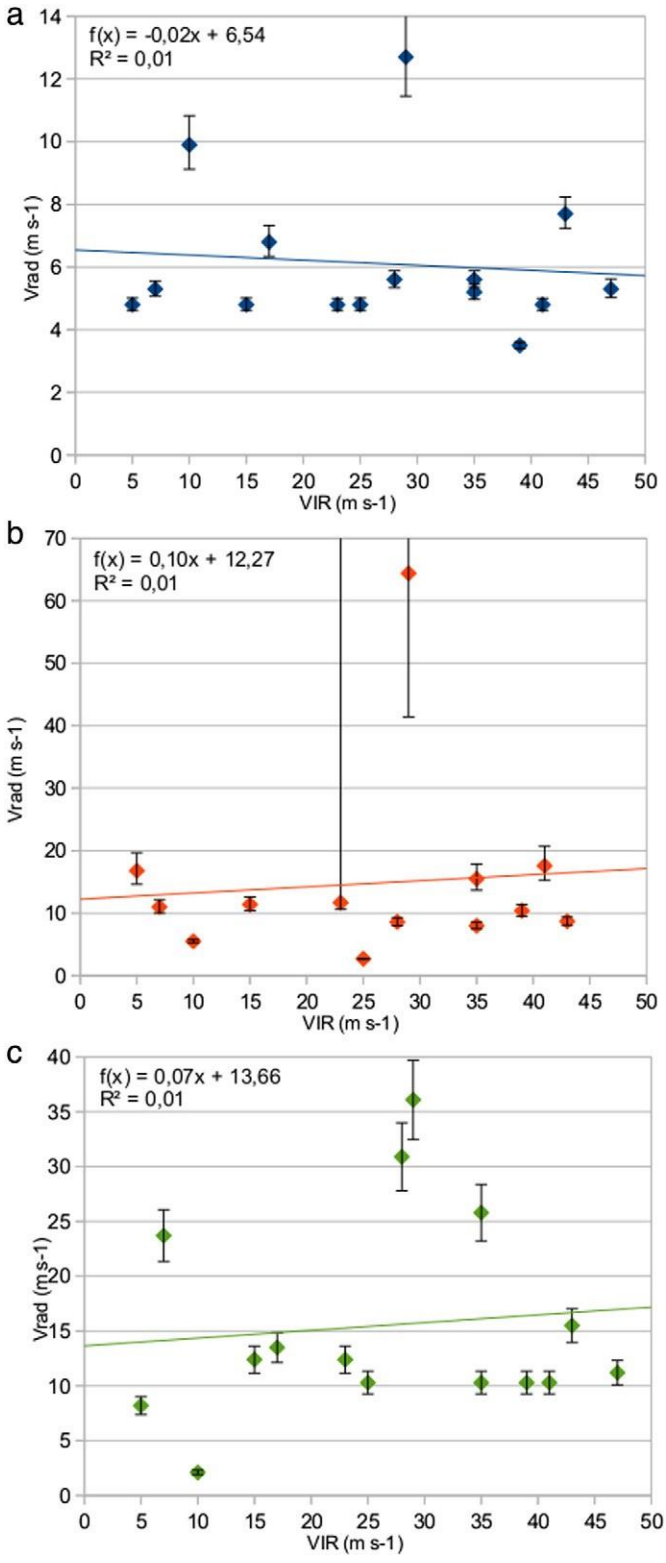

Fig. 4. Velocity estimated from currently used methods from radiometric signal waveform (Vrad) against velocity derived from infrared camera (VIR). a) Method using delay between onset and first inflexion point. b) Method using delay between onset points of two superposed radiometers. c) Derivative method.

responsible for the onset and first inflexion point of radiometric signal were moving between the spray and burst fronts as defined by Harris et al. (2012). Measured velocities of these parts of the plume in IR video frames range from 15 to 80 m s^{-1} for the burst (mean value of 31 m s^{-1}), and 18 to 123 m s^{-1} for the spray (mean value of 54 m s^{-1}). Like in previous studies (e.g., Taddeucci et al., 2012), we notice that the ejection velocity varies a lot during an eruption, including successive peaks attesting of repeated discharge pulses. For different thermal components of the same eruption, we were able to find values ranging from 17 to 83 m/s. All these values are within the range of values reported in the literature (e.g., Harris and Ripepe, 2007a,2007b; Harris et al., 2012). In comparison, maximum along-beam velocity components measured by a Doppler radar above the vent during the burst periods range between 40 and 134 m s^{-1} (peaks ≥ 170 m/s), with an average of 82 m s^{-1} (Fig.5a; Donnadieu, unpublished data). The 23-cmwavelength radar acquired at 24 Hz (for a description of VOLDORAD, see: Dubosclard et al., 2004; Donnadieu et al., 2005; Donnadieu, 2012) and aimed downward (beam bottom at −30°) to the vent from near the Pizzo. In this configuration, maximum vertical velocities (80–268 m s^{-1}, peaks ≥ 340 m/s) are about twice the radial component measured by Doppler effect from echoes of ascending particles. As the pixel resolution in our IR video frames was not sufficient to capture subcentimetric particles associated with the highest velocities, it is unsurprising that spatially better resolved methods record higher particle velocities in the range 200–405 m s^{-1} (Taddeucci et al., 2012; Bombrun et al., 2014), consistent with values inferred from the radar.

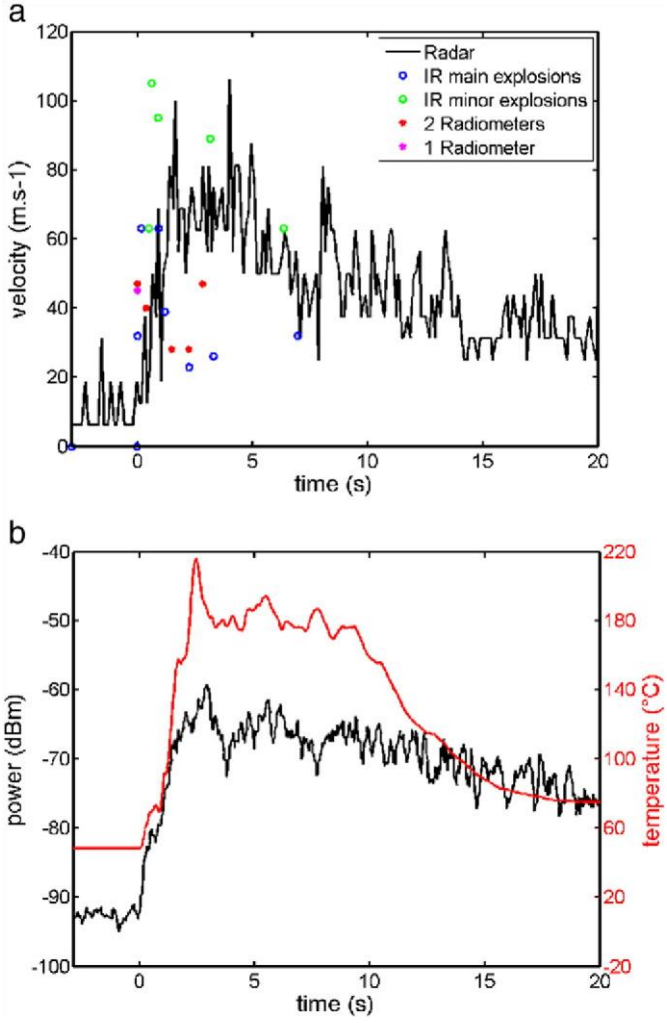

Fig. 5. Comparison of parameters retrieved from Doppler radar and radiometers (05/10/12, 10:57 UT, SW crater). (a) Velocity estimates retrieved from Doppler radar (along-beam; Donnadieu, unpublished data), infrared camera and radiometers. b) Radar power and radiometric thermal data are related to the particle concentration and size within their FOV, thus representing a proxy for the mass flux. The main explosive pulses are visible on both signals.

These results lead us to reconsider the definition of ejection velocity. Radiometric methods mainly characterize the external part of the plume

facing the sensor, all the more so where the plumes are thicker, denser, with a higher ash content, and hence opaque at IR wavelengths (e.g., Wen and Rose, 1994; Gouhier et al., 2012). Velocities calculated from radiometric methods deviate significantly from along-beam particle velocities measured by a Doppler radar inside the plume, just above the vent (Donnadieu, unpublished data). Defining a single ejection velocity above the vent for a Strombolian eruption appears to be irrelevant. In fact the plume is composed of several thermal components, with heterogeneous speeds, but not numerous enough to obtain representative values by averaging results. Improving velocity measurement precision in this case is only meaningful for a precise description of part of the eruptive event.

Velocity measurement from radiometric signal might then depend a lot on the method used and on the radiometer sensibility, and this has to be kept in mind. However, the results obtained from previous methods using radiometers remain very low compared with IR video values for the thermal component that cause radiometric signal onset. We thus exploit the video a bit further to identify possible error sources.

5.2. Error sources

By comparing radiometric signal with thermal video data, we identified several error sources that may limit velocity retrievals.

(i) The complexity of the eruption mechanism, and hence ofthe radiometric signals: IR videos reveal many discharge pulses, overlapping in time and space, jets inclined in various directions, with non-homogeneous, time-varying temperatures. Therefore the signal variations used to retrieve velocities can be not caused by the same (expected) plume component.

(ii) Field difficulty: exit vents were hidden by the crater rim. Anticipating the material exit direction can be very challenging, especially when the FOV size is not much bigger than the jet diameter and when aiming above the vent rather than precisely into the vent, as in our case. We found that inaccurate positioning of the radiometer FOV with respect to activity can be responsible for velocity underestimation by a factor of 2 (Fig. 6 and Table 2). In addition, as seen before, the complexity of 'simple' Strombolian eruptions leads to even greater errors in ejection velocity estimates.

(iii) Instrumental limitations: the radiometer's FOV may be not perfectly aligned with its aiming direction (0.5° here), causing inaccurate positioning. Both the radiometer and IR camera have a non-negligible response time (about 0.25 s for radiometers), and the recorded signal is smoothed and a bit staggered, which can be responsible for velocity underestimations.

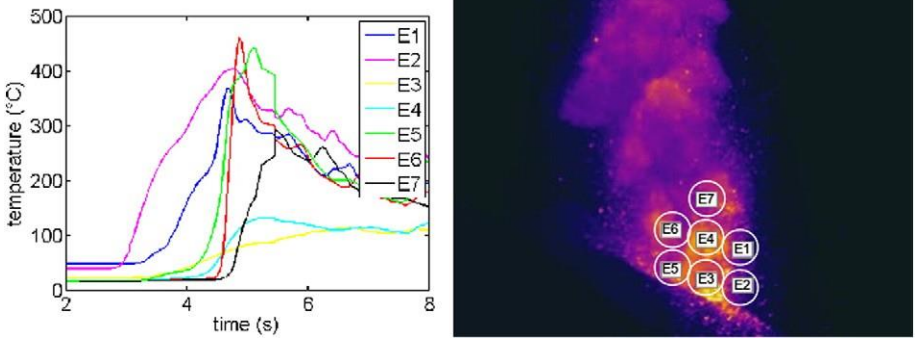

Fig. 6. Influence of FOV position (right) on radiometric signal (left). Positioning errors can cause the calculated velocity to be twice lower.

Whereas radiometer's aiming direction can be easily corrected with careful calibration, limiting the impact of some of these error sources would require more specific adaptation of the instruments and the estimation method. More accurate and faster responding radiometers exist (up to N100 Hz), however this would not be sufficient to deal with all the error sources we identified.

Table 2
Influence of radiometer FOV position on retrieved velocity (Fig. 6).

FOV	E1	E2	E3	E4	E5	E6	E7
V (m s^{-1})	6.62	7.50	3.93	3.93	4.70	9.70	13.23

5.3. Influence of FOV shapes on velocity retrieval

In the following discussion, we focus on radiometer FOV's shape adaptation possibilities. IR camera data provides us with spatiotemporal information on the thermal components responsible for radiometric signal variations, and their characteristics. We investigate below several possible shapes for the radiometers' FOVs, that we expect more adapted to these pieces of information, and more suited to tracking a Strombolian plume front and characterizing its velocities. This is only beneficial if the adapted radiometer fulfills certain basic conditions: (a) it is easy to use; (b) there are negligible effects of imprecise FOV positioning on velocity results; (c) no additional measurements should be needed for data interpretation; and (d) the radiometric signal also has to be easy to interpret and give reliable measurements.

5.3.1. Method: synthetic radiometric signal

To study the influence of a radiometer's FOV shape on radiometric signal, we calculated "synthetic" radiometric signals from IR video sequences, using the FLIR software ResearchIR. We defined an area corresponding to a radiometer FOV within the camera frame. ResearchIR offers simple options that allow to define elliptic or rectangular areas in the FLIR video images, and to follow the temperature evolution in this area during the whole movie. The areas we define here were designed to have FOV aperture angles of sizes comparable with real radiometers' FOVs. We then calculated the mean temperature value over this area for all the images of the video sequence. This temperature, averaged over several camera pixel sensors, should be comparable to the temperature that would have been recorded by a radiometer of corresponding FOV:

$$\sigma T_{rad}^4 = \int_{FOV} \sigma T^4(x,y)\,dx\,dy = \sum_{pix} \int_{FOV\,pix} \sigma T^4(x,y)\,dx\,dy \qquad (10)$$

We then use this synthetic radiometric signal for velocity estimations.

We here assimilate the plume front to the first particles that cross the radiometer's FOV, that is, for most of eruptions, the spray of the burst.

5.3.2. 15° FOV radiometer

15° FOV radiometers are often used in studies of volcanic activity, to couple the thermal data with seismic and acoustic data (Sahetapy-Engel et al., 2008). Because of their large FOVs, using such radiometers would be a first possibility to avoid aiming issues during field work. This could also potentially lead to more representative velocity estimations as the plume front could be followed over a longer distance, with less effects of the plume inclination.

5.3.2.1. Method. With this FOV size, the previous methods for velocity measurements can no longer be used, as those are adapted for smaller FOV radiometers. Here we use the relationship between signal variations and the FOV fractional area f occupied by the plume. Eq. (3) can be rearranged as:

$$f = \frac{T_{rad}^4 - T_c^4}{T_h^4 - T_c^4}. \quad (11)$$

For all eruptions analyzed, using synthetic data, the mean correlation coefficient between f and T_{rad}^4 is only 0.45, indicating that the main inherent assumption of constant and homogeneous temperature is certainly incorrect for the plume as a whole. Indeed, the application conditions are not fulfilled as the plume cools down. However, during the initial plume ascent, corresponding to the radiometric temperature increase phase, the mean correlation coefficient is 0.83, suggesting that the main assumption remains valid for the initial ascent phase. The correlation for an illustrative eruption is shown in Fig. 7, with an excellent linear fit to the data (r^2 = 0.99) during the ascent phase. We consider that all area variations are due to vertical movements (no radial expansion). This assumption is quite realistic for SW vent gas-rich eruptions, involving well collimated jets, although it may lead to over estimation of the plume front velocity. This time, df / dt theoretically remains the same during the ascent of the plume. We adapt Eqs. (8) and (9), using S = L/A where L is the plume width, and A is the FOV area.

Aiming at retrieving accurate velocity estimates with radiometric data alone requires values for T_h, T_c and L to be determined. However, measuring these variables in the field is highly challenging because of the brief eruption period, the poor visibility of the plume contours, etc. We instead use typical values for Strombolian eruptions: L = 20 m, T_h = 423 K, T_c = 293 K. Those values were estimated from IR videos, during the ascent of the first burst. T_h is the mean apparent temperature of the plume, resulting from sparse hot particles on a colder background.

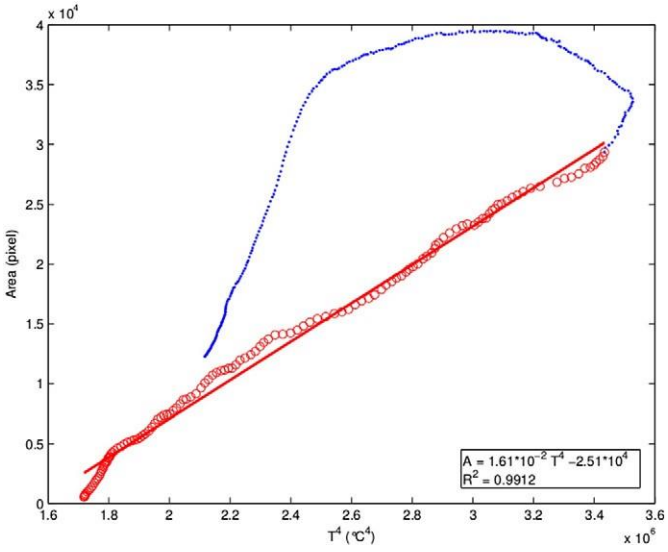

Fig. 7. Examples of temperature-area correlation for a 15° FOV radiometer during an eruption (SW crater, 27/09/12, 14:25 UT). Both occupied FOV fractional area f and synthetic radiometric temperature were measured for each FLIR video frame (30 Hz). f is well correlated with T^4 during the ascent phase (red circles) of the lava jet (linear fit is indicated), validating the two component description of the eruption (Eq. (11)) for the initial ascent phase. However, this assumption is no longer realistic for the rest of the eruption (blue points) due to cooling and scattering effects.

5.3.2.2. Results. The velocity values obtained with the synthetic signals were all lower than 10 m s^{-1}, which is even lower than those obtained from the actual radiometric signals, and clearly unrealistic. Obviously the error made using typical values is too big and the assumptions of a single emission with no temperature variations are too loose.

5.3.3. Single radiometer with rectangular FOV

The radiometers generally used are not well suited for velocity estimations in the configuration of Stromboli volcano. The FOV shape has to be more specifically adapted to the eruptive plume characteristics. Respecting conditions raised in Section 5.3 means knowing exactly which plume movements in the FOV cause the signal variations. This is only possible if the new radiometer is adapted to tracking a precise part of the plume, which exists in every eruption and is easy to follow. We thus firstly focus on the top part of the plume as this part of the plume was observed to be relatively homogeneous in temperature and diameter over a few meters, particularly in gas-rich eruptions. We then discuss how representative this could be of the whole plume. The radiometers' FOVs we experiment here are purely theoretical. We tested various configurations to find the best way to adapt actual radiometers for eruption monitoring.

5.3.3.1. Method. The first radiometer configuration to be experimented with is a rectangular-shaped FOV with a high width/height aspect ratio as that presented in Fig. 8. Its greater width limits horizontal positioning problems. It is centered close to the vent, where the plume front movement is likely to be mostly vertical, hence with limited horizontal component of particles' ballistic trajectories at this stage. So the plume diameter can thus be considered constant. We tested vertical FOV aperture angles ranging from 0.4 to 3°, in order to find the best compromise for temperature homogeneity and quality of the data for Stromboli's 'normal' explosions. Thermal homogeneity is essential for signal interpretation and constrains the FOV's height as it must encompass the upper part of the plume and be sufficiently small to limit cooling effects. The FOV needs to extend high enough vertically with respect to the ejection velocity to accurately pick up the signal variations. The expected radiometric signal is presented in Fig. 9 (a, b). As the plume fronts are generally not sharp in reality, owing to the spray of small particles (generally sub-pixelar and much faster than the instrument's response time) ahead of the main burst, the signals differ from the ideal case in Fig. 9, with onset and inflexion points less constrained in time and temperature. Radiometers with a vertical aperture angle of 1° record good quality data, and meet the temperature homogeneity assumption for most cases.

For a FOV height of 1°, data points were too poorly-constrained to use the time delay calculation methods. Instead, we develop and investigate below the potential application of a method based on the signal derivative from a radiometer with a rectangular FOV and 1° vertical aperture. Considering that the plume width is constant when it crosses the radiometer, the rectangular shape of the FOV provides a simplification for the calculation. Indeed, a plume of width L and temperature T_h crossing the rectangular FOV with width D induces the same signal as a plume of the same speed, width D, and temperature T_2 (Fig. 10), where T_2 is:

$$T_2 = \frac{T_h L + T_c (D - L)}{D}. \quad (14)$$

T_c is the temperature recorded by the radiometer before the plume enters its FOV. T_2 is the temperature recorded when the plume front exits the FOV, which appears as a slope break in the radiometric signal (Fig. 10). We again use Eqs. (8) and (9), with this time S = 1/H, H being the vertical extension of the FOV above the vent.

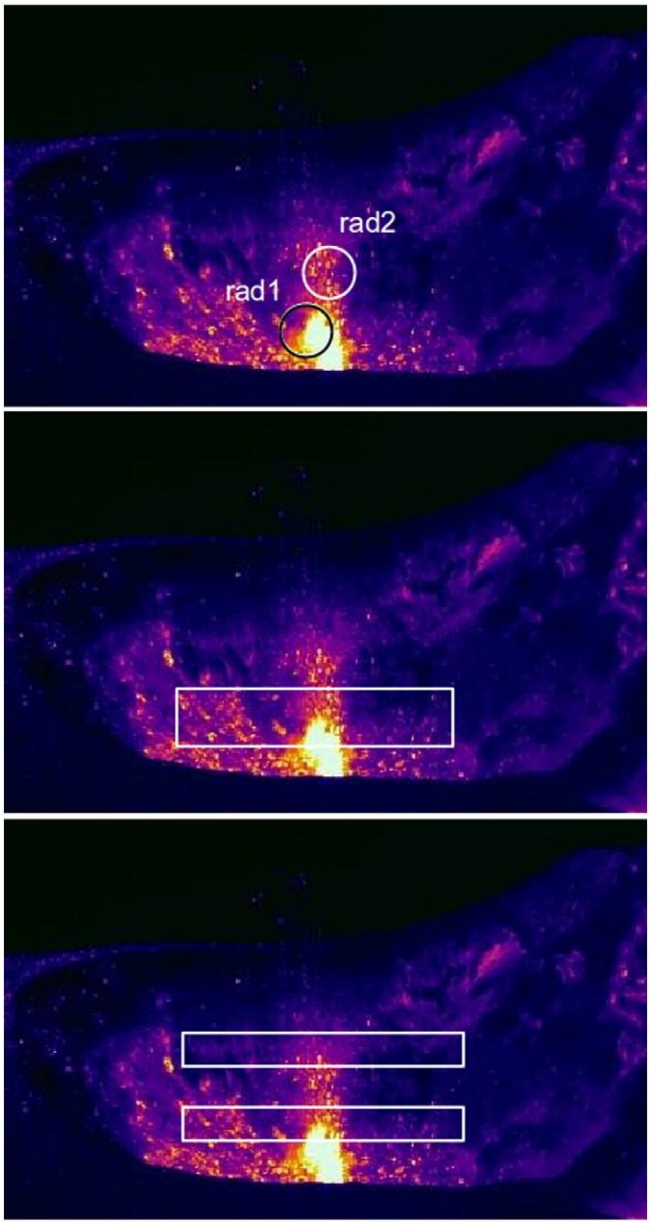

Fig. 8. Radiometers' FOVs tested: (a) 1° FOV radiometer (like those used in this study); (b) single rectangular FOV radiometer (FOV's height 1°, see text); (c) superposed rectangular FOV radiometers (FOVs' height 0.75°, distance between FOVs 1.5°, see text).

5.3.3.2. Results. We performed the velocity calculations on synthetic radiometric signals obtained with a 1 × 5.5° FOV radiometer for the eruptions recorded in the same configuration at the SW crater, for which the plumes were well-collimated jets with little air entrainment, and the initial spray of particles was clearly visible. We also performed these calculations for buoyantly rising plumes from the NE crater. Results were compared with velocity values measured on corresponding IR videos (supplementary material 3). These velocity values were calculated using the time needed for the front of the plume, defined as the first hot particles detected in the thermal video, to cross the FOV in the IR video. The error was quite large (up to 50%) due to the rapidity of this FOV crossing (sometimes no more than 0.4 s, i.e., 2 video frames).

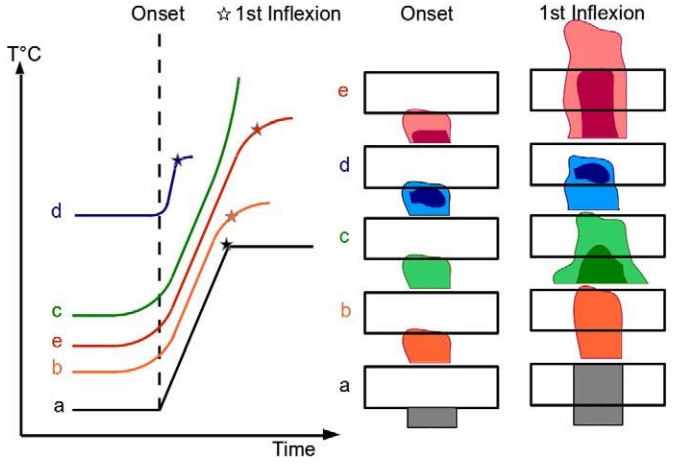

Fig. 9. Complex interpretation of onset and inflexion points in radiometric signals. (a) Ideal signal. (b) Theoretical interpretation of onset and inflexion points of a typical signal during plume emission. (c) Exception 1: the arrival of a hotter component (dark green) in the FOV masks the first inflexion point. (d) Exception 2: a small hot component (dark blue) produces a fast increase and a sooner inflexion point. Calculated velocity associated to this variation is higher than the real velocity. (e) Exception 3: fast diffuse first particles produce the same temperature variation as a slower hotter component (dark red), the first inflexion point comes later. Calculated velocity is then smaller. This case is close to case (c). All these exceptions result from the influx into the FOV of a hot component, which is not constant due to spatiotemporal temperature inhomogeneity and plume diameter variations.

Synthetic velocities calculated with this method agree reasonably well with the values measured on the IR video (Fig. 11), despite the departure of a few data points from the general trend. For the recorded eruptions, the mean normalized difference from IR values is of only 25%. The sensitivity of the method to velocity variations is good, as the signal characteristics used do not depend on the acquisition limits of the camera. However, after applying this method to the more complex dynamics of the NE crater eruptions, involving oriented successive pulses with ash and bombs, we had to reconsider the validity of the signal interpretation. Indeed, results for the NE crater eruptions were poorly correlated with the observations. The temperature and diameter variations at the top of the plume front were fairly large, and part of the signal variations was hidden. The onset and inflexion points were actually caused by hot plume components entering successively into the FOV, associated with flux variations. Temperature inhomogeneity, and the different velocities of the plume components added unexpected signal variations that masked those associated with the plume front. Several examples of complex signal are presented in Fig. 9 (c–e).

This single radiometer method, like most current radiometric methods, aims to provide global characteristics of the plume dynamics, assuming that the plume is thermally homogeneous enough and has simple dynamics. This approach is relevant for two cases: (i) when the eruption is close to an ideal case: the plume is homogeneous both in temperature and speed, and has a sharp front; (ii) when the plume is not thermally homogeneous, but its width is much greater than the typical dimension of its heterogeneities. In this case, the turbulent dynamics of the plume remain well-described by simple models using averaged values. The heterogeneities statistically vanish and the average is representative of the whole plume.

The single rectangular FOV radiometer method we propose makes it possible to use this kind of approach for cases with heterogeneous plumes of about the same size as thermal heterogeneities. This method allows the evolution of a specific part of the plume to be followed within the FOV. By adapting the FOV shape to the characteristics of the observed activity, a thermally homogeneous component of the plume can be focused on, leading to reliable velocity values for this part of the plume. However, as soon as the conditions for homogeneity of the thermal component are not satisfied, or when thermal pulses overlap within the FOV, the results become unreliable. Besides, adaptation to the size of heterogeneities is limited by the competitive constraint of

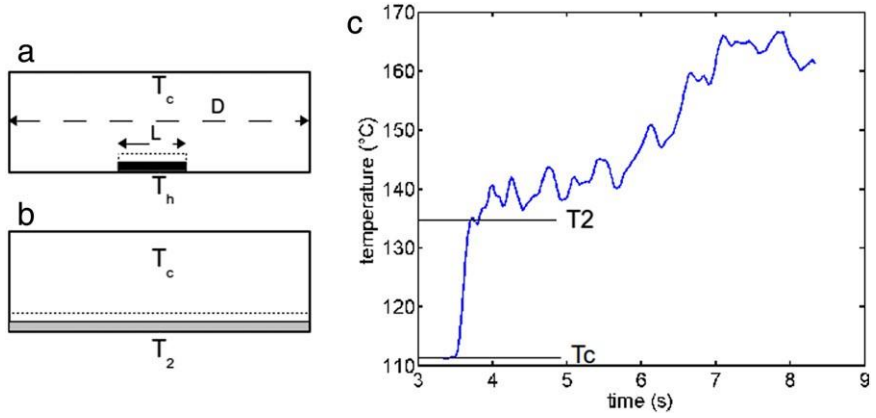

Fig. 10. Calculation method for single rectangular-shaped radiometer. (a) The real plume of temperature T_h and width L generates the same temperature variations as a plume of temperature T_2 and width D (b). (c) T_c and T_2 can be measured on radiometric signal.

crossing time, which has to be high enough to obtain reliable velocity estimation.

We thus experimented a second method, using two superposed rectangular radiometers. This way we focus on the propagation of the temperature signal, and circumvent the temperature homogeneity constraint for the plume.

5.3.4. Superposed rectangular radiometers

5.3.4.1. Method. The second method we experimented with was based on the delay time between signal onset points from two superposed rectangular FOVs. The shape of these FOVs is almost the same as for the single FOV. However, with the delay time method used here, we only track the very front of the plume, then homogeneity for the plume is not required. For thermally homogeneous plumes, results from this method should be comparable with results from single radiometers methods. However, for heterogeneous plumes, this method provides insight into vertical velocity variations within the plumes, by following the propagation of successive signal variations.

The relative vertical positions of the FOVs need this time to be known precisely. For the next field measurements, the two radiometers could be fixed together, and the relative FOV positions should be calibrated. Using IR videos and ResearchIR analysis to calculate synthetic radiometric signals, we again centered on – and positioned the FOVs close to – the vent in order to exploit the vertical movement of the plume front. The two signals calculated for the same eruption were similar, attesting that the same thermal component was tracked, which should

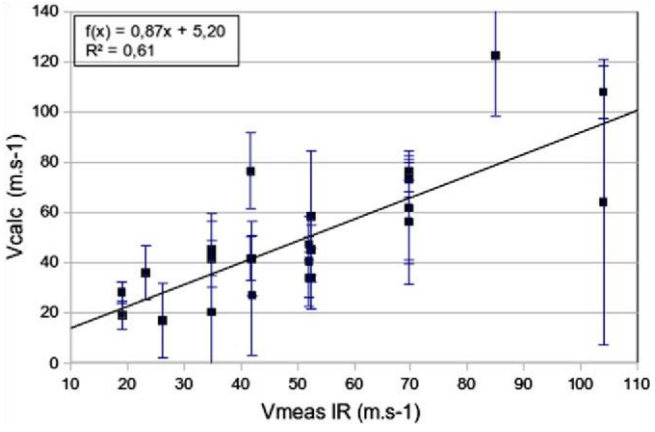

Fig. 11. Velocity calculated from the rectangular FOV synthetic signal (V_{calc}), compared to values measured on thermal videos (V_{meas} IR). Results are in good agreement, although the error can be very important.

lead to more reliable results. The major source of error here is the time resolution, and the time precision of onset and inflexion points picked. We used FOVs with a smaller vertical aperture angle than before (0.75°), to get sharper variations, hence a potentially better precision. The FOVs used are presented in Fig. 8 and the angular distances tested between FOVs were 1.5 and 3°. We performed velocity calculations for the eruptions that occurred on the 27 September and on the 3, 4 and 5 October 2012.

5.3.4.2. Results. Results from the method with superposed radiometers were reasonably good, despite some scattering (Fig. 12). However, the precision for velocity estimation was poor. For the recorded eruptions, the mean normalized difference from IR values is this time of 39%. The time taken by the plume front to cross the consecutive FOVs corresponds to a very small number of video frames, from which the synthetic signal is calculated, which results in poor velocity sensitivity and large errors on the results (up to 30%). More distant radiometers induce less data point scattering, but velocity values synthesized in this way are lower, due to plume deceleration (Fig. 12a). In addition, the onset point is sometimes hard to define. This is not only due to the camera acquisition frequency, but also to the fact that the plume front is less hot, more diffuse, and induces only a small thermal variation. This variation is averaged over the whole FOV, and thus appears even lower on the signal. Results from radiometers with smaller vertical aperture angles are not much better (Fig. 12b). Indeed, the non-sharpness of the plume front causes the onset point to spread. Improving precision of the onset point highlights the influence of the very first, fastest particles. This explains the higher velocity values sometimes obtained. The plume front speed thus appears not to be homogeneous.

The method using two radiometers, however, gives a much better description and more robust interpretation of the plume front progression and dynamics than the method with a single radiometer, as signals allow the thermal anomaly propagation to be followed. This method also enables several successive thermal plume components to be followed (Fig. 13), in addition to the plume front. This gives a precise description of velocity evolution within the plume.

6. Conclusion

Although velocity estimations from radiometric signal would hardly be comparable with results from infrared video, the results obtained with the two methods we have developed are reliable enough to consider the use of radiometers for volcano monitoring, or to retrieve plume front speed estimates.

For Strombolian eruptions, the two methods could be combined to improve the description of the eruption and the velocity estimation. A good understanding of the eruption dynamics can be deduced from

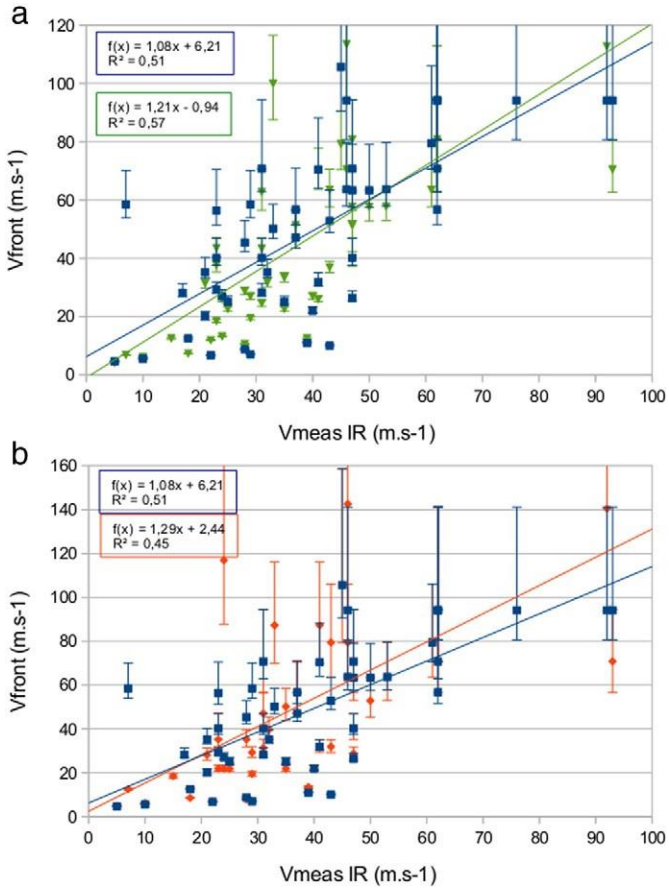

Fig. 12. Velocity calculated from delay time between the onsets of synthetized signal from two superposed radiometers. (a) Effect of separation angle between radiometers FOV axes (3° in green, 1.5° in blue); (b) Effect of FOV vertical aperture (0.37° in blue, 0.75° in orange). More distant radiometers give more reliable results, whereas FOV's height has little influence.

the method with superposed infrared radiometers, leading to a first approximation of the plume top velocity. As this method is also sensitive to the vertical thermal evolution within the plume, and knowing the plume velocity, it could provide information on the size of the plume's thermal components. The radiometric signal from the window radiometer method could then be analyzed to estimate more precisely the velocity of the plume components which satisfy the conditions of homogeneity.

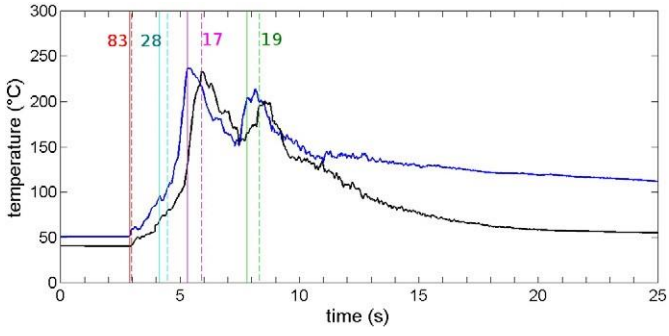

Fig. 13. Thermal signature from two superposed radiometers (lower one in blue) at Stromboli SW crater (05/10/2012, 13:45 U.T.). Velocities values (m/s) calculated from the signal delay are indicated. They depend strongly on the thermal component tracked.

We used synthetic data here, obtained from IR videos whose frame frequency is 30 Hz. Usual radiometers have an effective accuracy of the order of 0.1 s only, and commonly a response time of 0.2 to 0.5 s (e.g., Cyclops 300 AF). This causes the signal variations to be less sharp. We estimated that velocity values calculated from the signals from such radiometers could underestimate real velocities by a factor of 2. However, more accurate and faster responding radiometers exist (up to 1000 Hz like Mikron MI-GA in SW-IR, or some Chino or Omega sensors in broad-band IR; for technical characteristics, see for example Harris, 2013) that are compatible with magmatic temperature measurements and should give more precise velocity measurements of the ascent of individual thermal components of the plume. As long as the rate of change in the signal is less than the instrument slew rate (maximum rate of change of the output voltage), the onset and inflexions should be recorded at the correct time. According to Harris (2013), errors decline to around 1% for thermal variations developing over five times the response time (i.e., a few ms for fastest responding radiometers). While such high-rate measurements would provide access to processes at much smaller time-scales, the latter might also lead to new complications in signal interpretation. Data processing could also be improved by integrating the exact instrument response laws to eruption-like thermal variations, which could be experimented in the lab. The radiometers we tested here are not available for sale. However, rectangular FOV radiometers already exist (Apogee instruments for example). Besides, existing 15°FOV might be easily adapted to match this kind of configuration.

For Strombolian eruptions, velocity estimations from radiometric signals are not sufficient to define an ejection velocity estimation, as this is strongly dependent on specific thermal plume components. However, they facilitate a description of the plume's velocity, and the eruption dynamics. Velocity of the plume front can also be used as a qualitative proxy to determine the eruption style and energy. Indeed, low velocity values are associated with buoyantly rising plumes, which correspond to the ash-dominated plume-forming eruptions of type 2 (Ripepe et al., 1993, 2005; Patrick et al., 2007; Goto et al., 2014). High velocity values are associated with gas-thrust jet dynamics, characteristic of the gas-driven ballistic ejection without significant ash of type 1, or type 3. The latter type was recently characterized by Goto et al. (2014) as jet-like eruptions, gas-rich, highly energetic, and longlasting (15–20 s), producing high pressures (sometimes shockwavelike) with much higher-frequency (N200 Hz) audio component. Although less information can be retrieved from radiometers than from thermal cameras, radiometers are much less expensive and can still provide a proxy for the erupted mass, including successive pulses (Fig. 5b), as well as velocity estimates of particular thermal components of a plume under the conditions emphasized in this paper. Radiometers may also be usefully combined with other instruments monitoring surface activity, such as radars, to document in more detail the dynamics of eruptive plumes, or with seismic or acoustic sensors, to infer on conduit processes.

Supplementary data to this article can be found online at http://dx.doi.org/10.1016/j.jvolgeores.2015.06.022.

Acknowledgments

We thank two anonymous reviewers for their constructive comments and Pr. Wilson for handling the manuscript. The data acquisition at Stromboli was funded by the Observatoire de Physique du Globe de Clermont-Ferrand (Action Spécifique 2012), the Chaire d'Excellence de la Région Auvergne of A. Harris, and CNRS-INSU program TerMEx MISTRALS AO2012-737781 (PI: FD). LC, now at University de Savoie, thanks Laboratoire Magmas et Volcans at Clermont University for facilities in the research work. We are grateful to P. Freville, C. Hervier and T. Latchimy for their help in material preparation, S. Valade and M. Bombrun for operating the thermal camera in the field and for providing movies. A. Harris is much acknowledged for useful discussions in the initial stage of the work. We are also much indebted to M. Ripepe, Dario Delle Donne, Georgio Lacanna, C. Hervier, P. Labazuy, and K. Kelfoun for their help in the field. We thank the Italian Civil Protection (DPC, Roma) for granting permission for operations in the summit area, and to COA (Stromboli) for overseeing helicopter

operations plus access control and safety during the experiment. We thank T. Stachowicz and V. Christmann for processing of radar data and discussions and F. Van Wyk de Vries for language improvement. Part of the research was financed by the French Government Laboratory of Excellence initiative n°ANR-10-LABX-0006, the Région Auvergne and the European Regional Development Fund. This is Laboratory of Excellence ClerVolc contribution number 165.

References

Blackburn, E.A., Wilson, L., Sparks, R.S.J., 1976. Mechanisms and dynamics of Strombolian activity. J. Geol. Soc. 132, 429–440.

Bombrun, M., Harris, A., Gurioli, L., Battaglia, J., Barra, V., 2014. Anatomy of a Strombolian eruption: inferences from particle data recorded with thermal video. J. Geophys. Res. Solid Earth 120, 2367–2387.

Carazzo, G., Kaminski, E., Tait, S., 2008. On the dynamics of volcanic columns: a comparison of field data with a new model of negatively buoyant jets. J. Volcanol. Geotherm. Res. 178, 94–103.

Chouet, B., Hamisevicz, N., McGetchin, T.R., 1974. Photoballistics of volcanic jet activity at Stromboli, Italy. J. Geophys. Res. 79 (32), 4961–4976.

Donnadieu, F., Dubosclard, G., Cordesses, R., Druitt, T.H., Hervier, C., Kornprobst, J., Lénat, J.-F., Allard, P., Coltelli, C., 2005. Remotely monitoring volcanic activity with groundbased Doppler radar. Eos 86 (21), 201–204.

Donnadieu, F., 2012. Volcanological applications of Doppler radars: a review and examples from a transportable pulse radar in L-band. In: Bech, J., Chau, J.L. (Eds.), In "Doppler Radar Observations - Weather Radar, Wind Profiler, Ionospheric Radar, and Other Advanced Applications" 409-446 ISBN: 978-953-51-0496-4.

Dubosclard, G., Donnadieu, F., Allard, P., Cordesses, R., Hervier, C., Coltelli, M., Privitera, E., Kornprobst, J., 2004. Doppler radar sounding of volcanic eruption dynamics at Mount Etna. Bull. Volcanol. 66, 443–456.

Gerst, A., Hort, M., Kyle, P.R., Vöge, M., 2008. 4D velocity of Strombolian eruptions and man-made explosions derived from multiple Doppler radar instruments. J. Volcanol. Geotherm. Res. 177 (3), 648–660.

Goto, A., Ripepe, M., Lacanna, G., 2014. Wideband acoustic records of explosive volcanic eruptions at Stromboli: new insights on the explosive process and the acoustic source. Geophys. Res. Lett. 41, 3851–3857.

Gouhier, M., Harris, A.J.L., Calvari, S., Labazuy, P., Guéhenneux, Y., Donnadieu, F., Valade, S., 2012. Lava discharge during Etna's January 2011 fire fountain tracked using MSGSEVIRI. Bull. Volcanol. 74, 787–793.

Harris, A.J.L., 2013. Thermal Remote Sensing of Active Volcanoes, A User's Manual. Cambridge University Press (736 pp.).

Harris, A.J.L., Ripepe, M., 2007a. Synergy of multiple geophysical approaches to unravel explosive eruption conduit and source dynamics — a case study from Stromboli. Chem. Erde Geochem. 67, 1–35.

Harris, A.J.L., Ripepe, M., 2007b. Temperature and dynamics of degassing at Stromboli. J. Geophys. Res. 112, B03205.

Harris, A.J.L., Ripepe, M., Hughes, E.A., 2012. Detailed analysis of particle launch velocities, size distributions and gas densities during normal explosions at Stromboli. J. Volcanol. Geotherm. Res. 231–232, 109–131.

Harris, A.J.L., Valade, S., Sawyer, G., Donnadieu, F., Battaglia, J., Gurioli, L., Kelfoun, K., Labazuy, P., Stachowicz, T., Bombrun, M., Barra, V., Delle Donne, D., Lacanna, G., 2013. Modern multispectral sensors help track explosive eruptions. Eos 94 (37), 321–322.

Hort, M., Seyfried, R., Vöge, M., 2003. Radar Doppler velocimetry of volcanic eruptions: theoretical considerations and quantitative documentation of changes in eruptive behaviour at Stromboli, Italy. Geophys. J. Int. 154, 515–532.

James, M.R., Lane, S.J., Chouet, B.A., 2006. Gas slug ascent through changes in conduit diameter: laboratory insights into a volcano-seismic source process in low-viscosity magmas. J. Geophys. Res. 111, B05201.

Jaupart, C., Vergniolle, S., 1989. The generation and collapse of a foam layer at the roof of a basaltic magma chamber. J. Fluid Mech. 203, 347–380.

Johnson, J.B., Harris, A.J.L., Sahetapy-Engel, S.T.M., Wolf, R., Rose, W.I., 2004. Explosion dynamics of pyroclastic eruptions at Santiaguito Volcano. Geophys. Res. Lett. 31, L06610.

Kaminski, E., Jaupart, J., 2001. Marginal stability of atmospheric eruption columns and pyroclastic flow generation. J. Geophys. Res. 106, 21785–21798.

Mastin, L.G., Guffanti, M., Servranckx, R., Webley, P., Barsotti, S., Dean, K., Durant, A., Ewert, J.W., Neri, A., Rose, W.I., Schneider, D., Siebert, L., Stunder, B., Swanson, G., Tupper, A., Volentik, A., Waythomas, C.F., 2009. A multidisciplinary effort to assign realistic source parameters to models of volcanic ash–cloud transport and dispersion during eruptions. J. Volcanol. Geotherm. Res. 186, 10–21.

Parfitt, E.A., Wilson, L., 1995. Explosive volcanic eruptions — IX: the transition between Hawaiian style lava fountaining and Strombolian explosive activity. Geophys. J. Int. 121, 226–232.

Patrick, M.R., Harris, A.J.L., Ripepe, M., Dehn, J., Rothery, D.A., Calvari, S., 2007. Strombolian explosive styles and source conditions: insights from thermal (FLIR) video. Bull. Volcanol. 69, 769–784.

Ripepe, M., Gordeev, E., 1999. Gas bubble dynamics model for shallow volcanic tremor at Stromboli. J. Geophys. Res. 104 (B5), 10639–10654.

Ripepe, M., Rossi, M., Saccorotti, G., 1993. Image processing of explosive activity at Stromboli. J. Volcanol. Geotherm. Res. 54, 335–351.

Ripepe, M., Harris, A.J.L., Carniel, R., 2002. Thermal, seismic and infrasonic evidences of variable degassing rates at Stromboli volcano. J. Volcanol. Geotherm. Res. 118, 285–297.

Ripepe, M., Harris, A.J.L., Marchetti, E., 2005. Coupled thermal oscillations in explosive activity at different craters of Stromboli volcano. Geophys. Res. Lett. 32, L17302.

Rust, A., Cashman, K., 2004. Permeability of vesicular silicic magma: inertial and hysteresis effects. Earth Planet. Sci. Lett. 228, 93–107.

Sahetapy-Engel, S.T.M., Harris, A.J.L., Marchetti, E., 2008. Thermal, seismic and infrasound observations of persistent explosive activity and conduit dynamics at Santiaguito lava dome, Guatemala. J. Volcanol. Geotherm. Res. 173, 1–14.

Scharff, L., Hort, M., Harris, A.J.L., Ripepe, M., Lees, J., Seyfried, R., 2008. Eruption dynamics of the SW crater of Stromboli volcano, Italy. J. Volcanol. Geotherm. Res. 176, 565–570.

Taddeucci, J., Scarlato, P., Capponi, A., Del Bello, E., Cimarelli, C., Palladino, D.M., Kueppers, U., 2012. High-speed imaging of Strombolian explosions: the ejection velocity of pyroclasts. Geophys. Res. Lett. 39, L02301.

Taddeucci, J., Palladino, D.M., Sottili, G., Bernini, D., Andronico, D., Cristaldi, A., 2013. Linked frequency and intensity of persistent volcanic activity at Stromboli (Italy). Geophys. Res. Lett. 40, 3384–3388.

Weill, A., Brandeis, G., Vergniolle, S., Baudin, F., Bilbille, J., Fèvre, J.F., Piron, B., Hill, X., 1992. Acoustic sounder measurements of the vertical velocity of volcanic jets at Stromboli volcano. Geophys. Res. Lett. 19, 2357–2360.

Wen, S., Rose, W.I., 1994. Retrieval of sizes and total masses of particles in volcanic clouds using AVHRR bands 4 and 5. J. Geophys. Res. Atmos. 99 (D3), 5421–5431.

Wilson, L., 1980. Relationships between pressure, volatile content and ejecta velocity. J. Volcanol. Geotherm. Res. 8, 297–313.

Wilson, L., Self, S., 1980. Volcanic explosion clouds: density, temperature and particle content estimates from cloud motion. J. Geophys. Res. 85, 2567–2572.

Woods, A.W., 1995. The dynamics of explosive volcanic eruptions. Rev. Geophys. 33, 495–530.